VII International Conference on Computational Methods for Coupled Problems in Science and Engineering
COUPLED PROBLEMS 2017
M. Papadrakakis, E. Oñate and B. Schrefler (Eds)

INFLUENCE OF CURRENT AND FREQUENCY ON ELECTROMAGNETIC STIRRING IN CONTINUOUS CASTING OF STEEL

MARJAN MAČEK*, ROBERT VERTNIK*† AND BOŽIDAR ŠARLER*‡

* Laboratory for Simulation of Materials and Processes
Institute of Metals and Technology (IMT)
Lepi pot 11, SI-1000 Ljubljana, Slovenia
e-mail: marjan.macek@imt.si, web page: http:// http://www.imt.si/

† Štore Steel d.o.o., Quality and Development
Železarska cesta 3, SI-3220 Štore, Slovenia
e-mail: robert.vertnik@store-steel.si, web page: http://www.store-steel.si/

‡ Laboratory for Fluid Dynamics and Thermodynamics
Faculty of Mechanical Engineering, University of Ljubljana
Aškerčeva 6, SI-1000 Ljubljana, Slovenia
e-mail: bozidar.sarler@fs.ung-lj.si, web page: http://www.fs.uni-lj.si/

Keywords: Continuous casting, Electromagnetic stirring, Steel, Meshless methods.

Abstract.
The purpose of this paper is a multiphysics simulation of 3D temperature and velocity fields in continuous casting of steel under the influence of electromagnetic stirring by a combined meshless - finite element method approach. The transport phenomena are calculated by a meshless local radial basis function collocation technique and the magnetic force by the finite element method solver Elmer. The electromagnetic stirring increases the mixing in the molten steel. The thermal gradient is sharper and solidification is faster along the strand. The results are similar to other publications in the field. The local radial basis function collocation method is for the first time applied to 3D continuous casting problem with mold electromagnetic stirring.

1 INTRODUCTION

In continuous casting (CC) of steel, the molten metal is poured into the water-cooled mold, where it partially solidifies. Solidified shell is strong enough to withstand the ferrostatic pressure when it is pulled out from the mold. The mechanical properties of the product depend on many different variables ranging from billet chemical composition and size to process parameters such as cooling rate, casting speed, submerged entry nozzle (SEN) position and details of the fluid flow of the molten steel [1].

Many defects can occur in CC, such as surface defects, inclusions, and segregation, and may lead to unacceptable quality. In addition to the proper tuning of the casting parameters (temperature, velocity, primary and secondary cooling rate) electromagnetic stirring (EMS) is another instrument to achieve an enhanced quality. EMS promotes the columnar to equiaxed

transition, reduces segregation and improves the surface quality. Different positions of stirrer are possible, but most widely used is the mold electromagnetic stirring (M-EMS) since mechanical properties are mostly determined in the mold region [1, 2]. Since the optimal stirrer parameters are different for each plant, each casting machine has to be calibrated separately [3].

The fluid flow in CC was studied experimentally with water instead of steel, since it has a similar kinematic viscosity as molten steel, but is not suitable for electromagnetic stirring (EMS), since it is not conductive. There are some experiments with mercury but are not practical on an industrial scale. The experiments are usually used only to test new ideas and phenomena and not for parameter optimization [4]. Further, measurements during casting are not practical, if even possible, hence numerical models are of great necessity [1].

The first models for EMS were analytical or semi-analytical [4]. The first pure numerical models were made by Fujisaki [5]. Similar studies of modeling more complex geometries, closer to the industrial setting were made [6]. In recent years the discussed multiphysics field expanded drastically, which reflects in a vast number of publications regarding different stirrers, strand shapes and alloys [3, 7–9].

The majority of the mentioned works uses the finite element method for magnetic field calculation and the finite volume method for fluid flow, mainly with commercial software packages such as ANSYS Fluent. Another, a novel class of numerical methods are meshless methods, where the computational domain is discretized into nodes and a further topological connection between them, such as polygonization, is not needed. Local radial basis function collocation method (LRBFCM) [10], a class of meshless methods, was persistently developed for even more complex and realistic problems, eventually modeling macrosegregation and electromagnetic braking during CC of steel [11, 12]. Despite that one of the main advantages of the meshless methods are their simple implementation, irrespective of the number of dimensions, the first LRBFCM 3D calculation of CC is achieved only in 2016 [1]. There exists also other meshless methods (e.g. finite point method, diffuse approximate method, element free Galerkin method), but the present work model only 2D phenomena in CC [13, 14].

In this work, a 3D continuous casting model for finding a steady-state solution is presented for 18 cm×18 cm billet casting machine (Figure 1), installed in Štore-Steel plant. Because it incorporates the electromagnetic stirring and the strand curvature, the model has to incorporate the whole domain, in contrast to the previous 3D study, where due to the symmetry and lack of EM stirring, only one quarter can be modeled [1]. However, in this study, macrosegregation is not modeled.

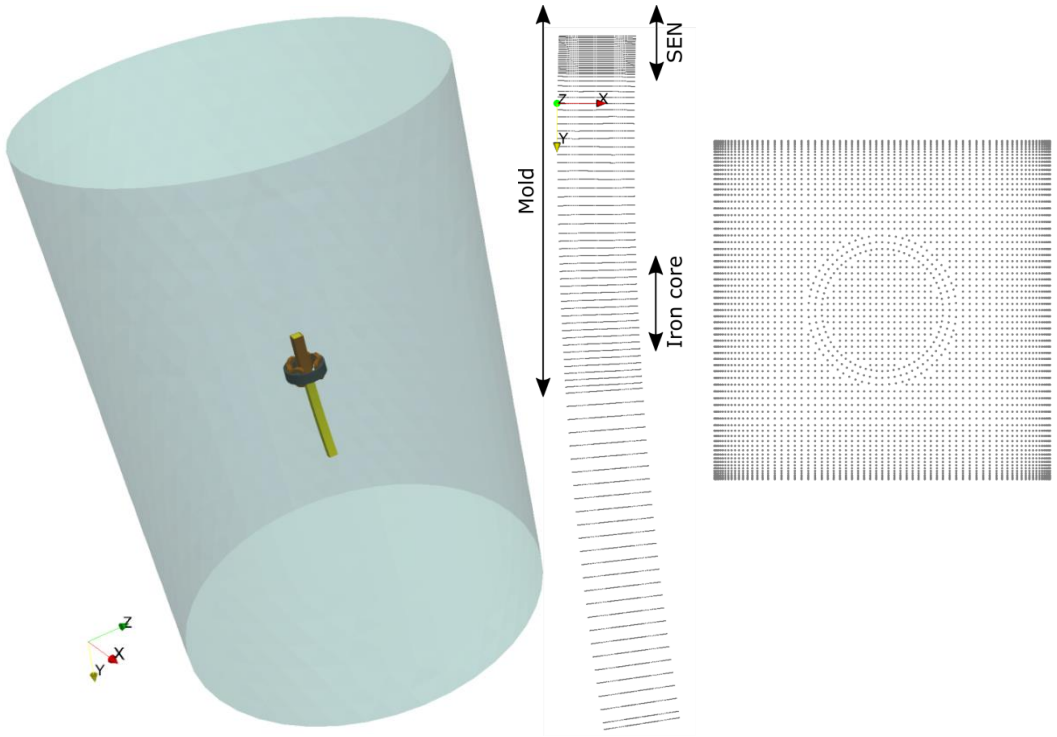

a) b) c)

Figure 1: Geometry used in the magnetic field calculation with the bounding air cylinder (a) and node distribution for casting calculation, where only the strand is modeled (b and c).

2 MAGNETIC STIRRING FORCE

The governing equations for electromagnetic field are

$$\nabla \times \mathbf{E} = -\frac{\partial \mathbf{B}}{\partial t} \tag{1}$$

$$\nabla \times \mathbf{B} = \mu_0 \mathbf{j} \tag{2}$$

$$\nabla \cdot \mathbf{B} = 0. \tag{3}$$

They are in the present work solved primarily with an open source finite element solver Elmer in **A**–V potential form, where the vector potential **A** is discretized into edge elements [15]. The equations (1)–(3) are solved in a frequency domain. Afterward, Lorentz force $\mathbf{f} = \mathbf{j} \times \mathbf{B}$ is calculated. The following assumptions are made [9]:

a) magnetic Reynolds number is small $R_\mathrm{m} = vL/\eta \ll 1$;
b) steel temperature is always above the Curie temperature;
c) the electrical conductance of solidified and molten steel is equal and constant;
d) characteristic time of magnetic force is much shorter than the fluid flow;
e) Joule heating $P = \int |j|^2 / \sigma \mathrm{d}V < 1\ \mathrm{kW}$ is ignored.

The magnetic Reynolds number stands for a ratio of magnetic advection and diffusion, where the magnetic diffusivity is $\eta = 1/\sigma\mu_0$. By inserting material properties of CC shows that the effect of conducting fluid flow is negligible, so a) is true. Because Curie temperature, below which the steel is ferromagnetic, is only about 750 °C (compared to casting temperature 1534 °C), almost no effect is expected since the calculations show that approximately only 0.2 % of the steel in the mold region is bellow Curie temperature. Nevertheless, the temperature profile in the strand has a strong effect on electrical conductivity σ. From the center of the strand to the mold, steel cools for about 700 °C with increasing σ for more than a factor of two. Because the temperature gradient is concentrated in the solidified zone, where the electric current $\mathbf{j}$ is the largest, it is questionable, if c) holds and has to be checked in future works. On the contrary, the temperature effect on the skin depth $\delta = (1/\sigma\omega\mu)^{1/2} \approx 0.3$ m in the strand is insignificant.

The characteristic time of the magnetic force is $1/2f < 0.3$ s, where f is current frequency, and characteristic time of the fluid flow is $L/u > 5$ s. The force has double the frequency of the electric current, since $|\mathbf{f}| \propto fB^2 \propto fI^2$. The assumption d) therefore allows a time-averaging of the Lorentz force to [4, 9]

$$\mathbf{f}_\mathrm{m} = (\mathbf{f}_\mathrm{Re} + \mathbf{f}_\mathrm{Im})/2. \tag{4}$$

Together with the first three assumptions this completely decouples the calculation of the magnetic force from the thermo-fluid calculations.

Consequently, we can have two separate geometries and node arrangements (Figure 1). The first one is used for magnetic force calculation and models the strand, the mold, the stirrer and also the bounding cylinder of air in which $\mathbf{A}$ and V drop to zero, which is also the only boundary condition necessary for EM field calculation. The second node arrangement (only nodes) used for casting simulation contains only the strand.

3 FLUID FLOW

The governing equations for turbulent incompressible fluid flow and heat transport with solidification are [1]

$$\nabla \cdot \mathbf{u} = 0 \tag{5}$$

$$\rho\frac{\partial \mathbf{u}}{\partial t} + \rho\nabla\cdot(\mathbf{uu}) = -\nabla P + \nabla\cdot[2(\mu_\mathrm{L}+\mu_\mathrm{t})\mathbf{S}] - \frac{2}{3}\rho\nabla k - \mu_L K_0 \frac{(1-f_\mathrm{L}^2)}{f_\mathrm{L}^3}(\mathbf{u}-\mathbf{u}_\mathrm{S}) + \mathbf{f}_\mathrm{b} + \mathbf{f}_\mathrm{m} \tag{6}$$

$$\rho\frac{\partial h}{\partial t} + \rho\nabla\cdot(\mathbf{u}h) = \nabla\cdot(\lambda\nabla T) + \rho\nabla\cdot[f_\mathrm{S}(h_\mathrm{L}-h_\mathrm{S})(\mathbf{u}-\mathbf{u}_\mathrm{S})] + \nabla\cdot(f_\mathrm{L}\frac{\mu_\mathrm{t}}{\sigma_\mathrm{T}}\nabla h_\mathrm{L}), \tag{7}$$

which represent mass, momentum and energy conservation, respectively. In the equations u, P, h and T stand for velocity, pressure, enthalpy and temperature. $\mathbf{S}$ is the strain rate tensor. Boussinesq buoyancy force is $\mathbf{f}_\mathrm{b} = \rho[\beta_T \mathbf{g}(T - T_\mathrm{ref})]$, where β_T stands for the thermal expansion coefficient. The magnetic force $\mathbf{f}_\mathrm{m}$ is inserted from (4). Density ρ, morphology constant K_0 in the Darcy term and dynamic viscosity μ are considered constant, but the thermal conductivity $\lambda(T)$ has temperature dependence.

The turbulence is modeled with $k-\epsilon$ turbulence model by using Abe-Kondoh-Nagano (AKN)[16] closure coefficients and put into effect with the third term on RMS in (6) and (7) with effective viscosity $\mu+\mu_\mathrm{t}$, where the turbulent dynamic viscosity is

$$\mu_\mathrm{t}=\rho c_\mu f_\mu \frac{k^2}{\epsilon}. \tag{8}$$

The turbulent kinetic energy k and the dissipation rate ϵ are determined from equations

$$\rho\frac{\partial k}{\partial t}+\rho\nabla\cdot(\mathbf{u}k)=\nabla\cdot\left[\left(\mu_\mathrm{L}+\frac{\mu_\mathrm{t}}{\sigma_k}\right)\nabla k\right]+P_k-\rho\epsilon+\rho D+\mu_\mathrm{L}K_0\frac{(1-f_\mathrm{L}^2)}{f_\mathrm{L}^3}k, \tag{9}$$

$$\rho\frac{\partial \epsilon}{\partial t}+\rho\nabla\cdot(\mathbf{u}\epsilon)=\nabla\cdot\left[\left(\mu_\mathrm{L}+\frac{\mu_\mathrm{t}}{\sigma_\epsilon}\right)\nabla\epsilon\right]+\rho\left(c_{1\epsilon}f_1-c_{2\epsilon}f_2\epsilon\right)\frac{\epsilon}{k}+\rho E+\mu_\mathrm{L}K_0\frac{(1-f_\mathrm{L}^2)}{f_\mathrm{L}^3}\epsilon, \tag{10}$$

where $c_\mu, f_\mu, c_{1\epsilon}, f_1, c_{2\epsilon}, f_2, \sigma_T, \sigma_k,$ and σ_ϵ are the closure coefficients. D and E are additional source terms of the low-Reynolds number turbulent model [17].

Solidification is modeled with lever rule liquid/solid fraction

$$f_\mathrm{L}=1-\frac{1}{1-k_\mathrm{p}}\frac{T-T_\mathrm{L}}{T-T_\mathrm{m}},\quad f_\mathrm{S}=1-f_\mathrm{L}, \tag{11}$$

where k_p is partition coefficient, T_L is liquidus temperature and T_m is melting temperature. Temperature is calculated from enthalpy $h(T)$ [1]

$$h_\mathrm{S}(T)=\int_{T_\mathrm{ref}}^{T}c_{p\mathrm{S}}\mathrm{d}T,\quad h_\mathrm{L}=h_\mathrm{S}(T)+\int_{T_\mathrm{S}}^{T}(c_{p\mathrm{L}}-c_{p\mathrm{S}})\mathrm{d}T+h_\mathrm{m}. \tag{12}$$

First, the equations (5) and (6) are solved by using Chorin fractional step method [14]. Then, h, k and ϵ are updated (7)–(10) with explicit time stepping. Finally, the new values of T, f_L and μ_t are calculated for each node. The steps are repeated until a steady-state is reached [1].

The meshless local radial basis function collocation method (LRBFCM) is employed for the numerical solution procedure. In each (overlapping) subdomain, the involved field Φ (e.g. temperature, pressure, velocity component, turbulent kinetic energy, turbulent dissipation rate) is represented by a set of radial basis function (RBF) $\psi(\mathbf{p})$, over K nodes positioned at nodes $\mathbf{p}_k$ in the subdomain

$$\Phi(\mathbf{p})=\sum_{k=1}^{K}\psi_k(\mathbf{p})\alpha_k. \tag{13}$$

The derivatives are considered with corresponding derivatives of $\psi_k(\mathbf{p})$. RBFs used in the present work are multiquadrics $\psi_k(\mathbf{p})=\sqrt{|\mathbf{p}-\mathbf{p}_k|^2+c^2}$, where c is the shape parameter. The elaboration of the method can be found in [18].

The boundary conditions at the inlet (i.e. SEN) are

$$u_{\text{inlet},x} = 0\frac{\text{m}}{\text{s}}, u_{\text{inlet},z} = 0\frac{\text{m}}{\text{s}}, u_{\text{inlet},y} = u_{\text{cast}}(a_b/d_2)^2, T_{inlet} = T_0, \frac{\partial P}{\partial y} = 0\frac{\text{N}}{\text{m}^2} \tag{14}$$

$$k_{inlet} = 1.5(I_t u_{\text{inlet},y})^2, \epsilon_{\text{inlet}} = \frac{c_\mu^{0.75} k_{\text{inlet}}^{1.5}}{0.07 d_2} \tag{15}$$

where I_t is the turbulent intensity

$$I_t = 0.16\text{Re}^{-1/8}, \quad \text{Re} = \rho u_{\text{inlet},y} d_2/\mu. \tag{16}$$

Pressure outlet with $P = 0\,N/\text{m}^2$ is prescribed at the outlet. Other variables are set to zero gradients in the vertical direction. On the top surface (i.e. meniscus), the free surface flow is prescribed with $u_y = 0\,\text{m/s}$.

On the side walls the boundary conditions for velocity are of the no-slip type if there is a liquid phase, or $u = u_{\text{cast}}$ is prescribed if the steel has solidified. For the heat transfer, Robin boundary conditions are used in the mold, where the heat transfer coefficient equals to $2000\ \text{Wm}^{-2}\text{K}^{-1}$. In the secondary cooling region, below the mold, the heat transfer coefficient equals to $800\ \text{Wm}^{-2}\text{K}^{-1}$.

4 RESULTS

The correctness of Elmer solver and the problem setup is verified on an analytical case (magnetic field of coils without the iron core) and on an axisymmetric case of DC aluminium casting, where the results are compared to those obtained from another open source finite element solver FEMM, which is intended for 2D electromagnetic problems [19]. The latter is also compared to our own meshless calculation too.

The vertical and the horizontal profiles for different frequencies and currents can be seen in Figure 2 and

Figure **3**. They roughly obey the dependency $|\mathbf{f}| \propto f I^2$, although they reach maximum intensity between 3 Hz and 5 Hz, after which the skin effect in the mold dominates over the frequency factor in $|\mathbf{f}|$. A strong spike is seen right at the bottom of the mold. This is because the stirrer is mounted right above the bottom of the mold (Figure 1), where the magnetic field should be still strong, but is shielded by the mold. The effect becomes stronger with higher frequencies, which further confirms the argument. This does not influence the stirring effect, because the force is in the vertical direction [8].

EMS has a dramatic effect on solidification shell and the effect on fluid flow is rotational, as expected (Figure 4). However, as noted in previous publications, the main effect is not due to swirling flow, but due to better mixing and thermal transport, resulting in a sharper temperature gradient along the strand [3]. It is clear that because of this, a particular cross section in the strand solidifies faster than without the stirring (a blunt solidification front in Figure 4 for EMS case).

The settings shown in the present paper are not optimal. As we can see in Figure 5 the rotational flow distorts the solidification front and makes the solidification non-symmetric. A

similar effect was found in literature [20]. It is expected, that this problem can be overcome by stronger stirring.

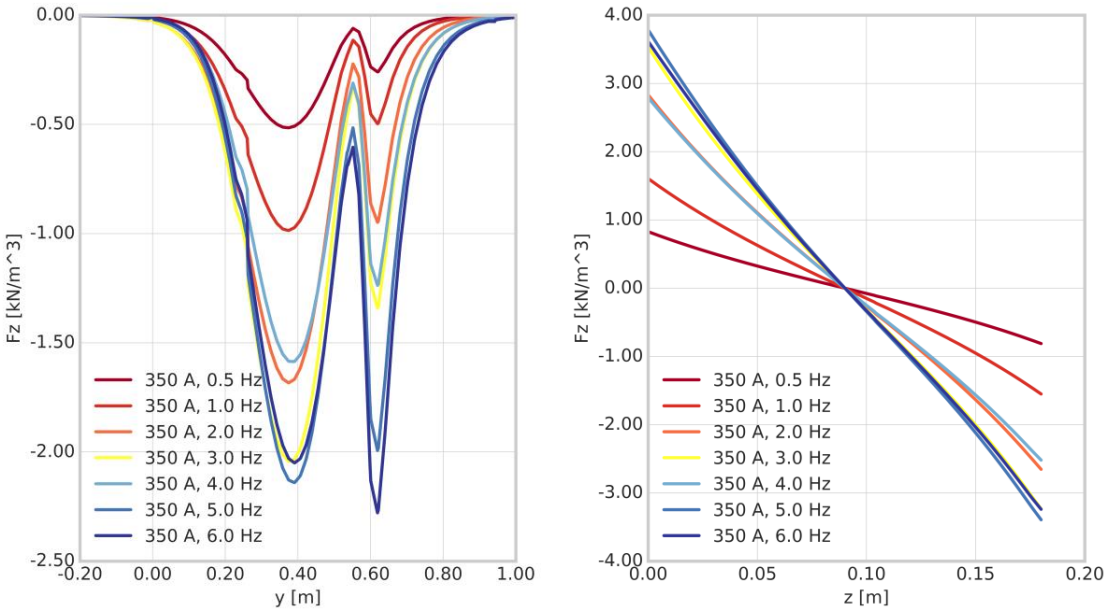

Figure 2: The magnetic force horizontal component z for different frequencies for vertical cross-section in the middle of the strand and 3 cm from the side (a) and in the horizontal cross section in the center of the EMS (b).

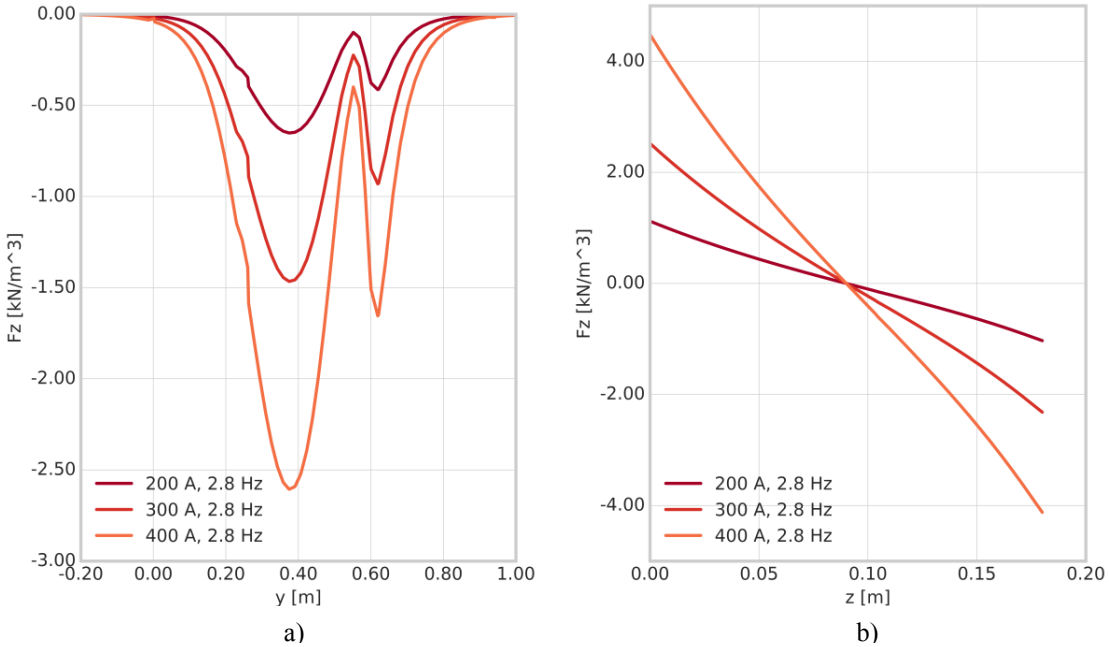

Figure 3: The magnetic force horizontal component z for different currents for vertical cross-section in the middle of the strand and 3 cm from the side (a) and in the horizontal cross section in the center of the M-EMS (b).

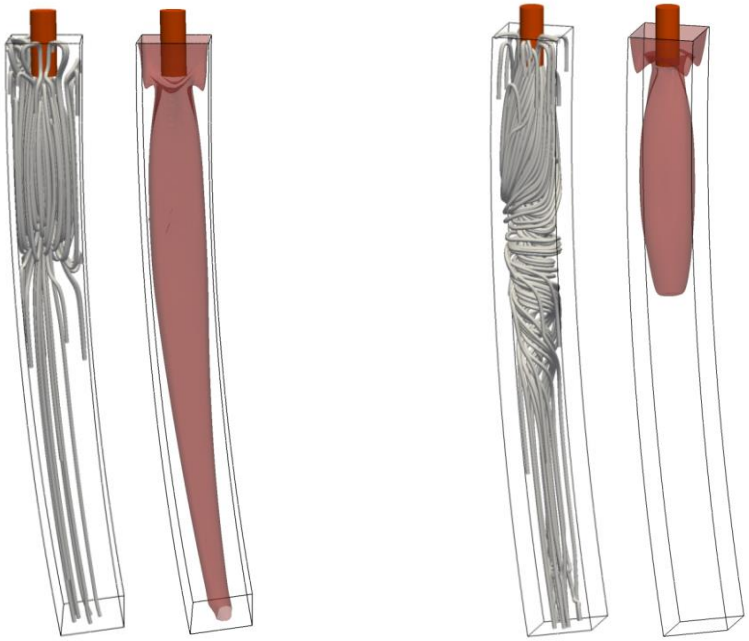

No EMS 300 A; 2.8 Hz

Figure 4: Streamlines and solidification front without and with EMS.

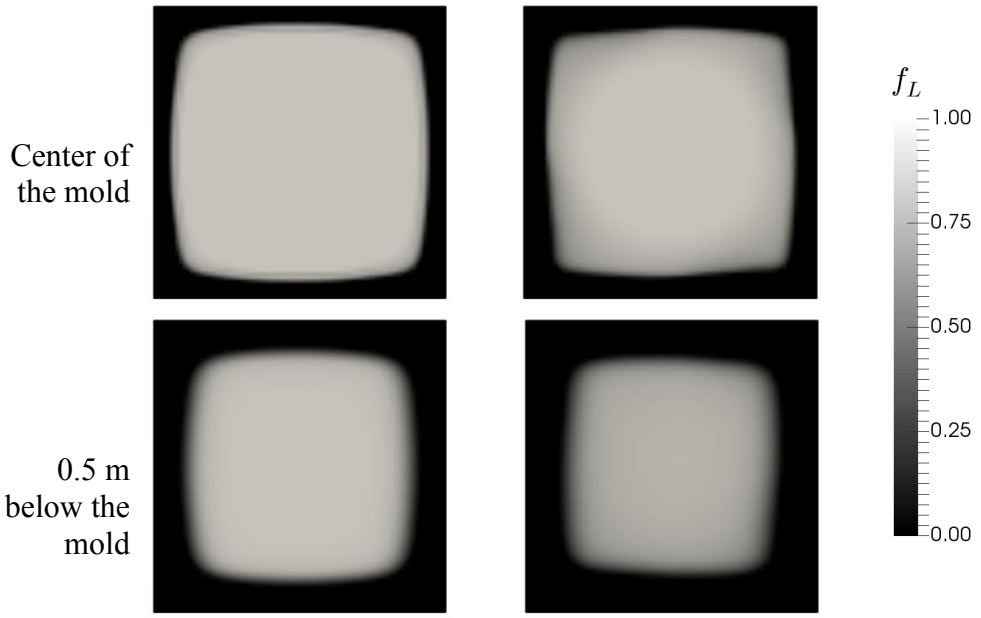

Figure 5: Liquid fraction without and with EMS for cross sections at the center of the stirrer and 0.5 m below it.

5 CONCLUSIONS

Lorentz force is successfully incorporated into the existing 3D meshless model of turbulent strand solidification and solved with LRBFCM in 3D. Due to the loss of symmetry the whole strand has to be considered and not only one quarter [1]. The obtained results are in accordance with those found in literature [7, 8, 20].

The calculation of the EM force with the use of a combination of our own meshes and open source finite element software is proven practical. Despite that, the challenge remains in efficiently connecting solvers for fully coupled problems. This is necessary, if one wants to study for example the effect of temperature dependence of electrical conductivity.

Challenges also remain in finding optimal stirring parameters for steel production and including macrosegregation and inclusion transport.

ACKNOWLEDGEMENTS

This work was funded by the Slovenian Grant Agency (ARRS) in the framework of applied research project L2-6775, co-sponsored by companies IMPOL and Štore-Steel.

REFERENCES

[1] Vertnik, R. and Šarler, B. Three dimensional simulation of macrosegregation in steel billets by a meshless method. *IOP Conf. Ser. Mater. Sci. Eng.* (2016) **117:**012069.
[2] Kunstreich, S. Electromagnetic stirring for continuous casting. *Rev. Métallurgie* (2003) **100:**395–408.
[3] Guo, Q., *et al*. Effect of Final EMS on Shrinkage Cavity of Bloom. *J. Iron Steel Res. Int.* (2015) **22:**93–97.
[4] Spitzer, K.-H., Dubke, M. and Schwerdtfeger, K. Rotational electromagnetic stirring in continuous casting of round strands. *Metall. Trans. B* (1986) **17:**119–131.
[5] Fujisaki, K. In-mold electromagnetic stirring in continuous casting. *IEEE Trans. Ind. Appl.* (2001) **37:**1098–1104.
[6] Trindade, L.B., *et al*., and Soares, R.B. Numerical model of electromagnetic stirring for continuous casting billets. *IEEE Trans. Magn.* (2002) **38:**3658–3660.
[7] Liu, H., *et al*. Numerical Simulation of Fluid Flow in a Round Bloom Mold with In-Mold Rotary Electromagnetic Stirring. *Metall. Mater. Trans. B* (2012) **43:**1657–1675.
[8] Geng, X., *et al*. Optimisation of electromagnetic field and flow field in round billet continuous casting mould with electromagnetic stirring. *Ironmak. Steelmak.* (2015) **42:** 675–682.
[9] Ren, B.-Z., *et al*. Numerical simulation of fluid flow and solidification in bloom continuous casting mould with electromagnetic stirring. *Ironmak. Steelmak.* (2015) **42:**401–408.
[10] Vertnik, R. and Šarler, B. Simulation of continuous casting of steel by a meshless technique. *Int. J. Cast Met. Res.* (2009) **22:**311–313.
[11] Vertnik, R., Šarler, B., and Senčič, B. Solution of Macrosegregation in Continuously Cast Billets by a Meshless Method. *IOP Conf. Ser. Mater. Sci. Eng.* (2012) **27:**012058.

[12] Mramor, K., Vertnik, R., and Šarler, B. A meshless model of electromagnetic braking for the continuous casting of steel. *Mater. Tehnol.* (2015) **49:**961–967.
[13] Košnik, N., *et al*. A multiphysics and multiscale model for low frequency electromagnetic direct-chill casting. *IOP Conf. Ser. Mater. Sci. Eng.* (2016) **117:**012052.
[14] Alizadeh, M., Jahromi, S. A. J., and Nasihatkon, S. B. Applying finite point method in solidification modeling during continuous casting process. *ISIJ Int.* (2010) **50:**411–417.
[15] 'Elmer 8.2'. [Online]. Available: https://csc.fi/web/elmer/elmer. [Accessed: 30-Mar-2017].
[16] Abe, K., Kondoh, T., and Nagano, Y. A new turbulence model for predicting fluid flow and heat transfer in separating and reattaching flows—I. Flow field calculations. *Int. J. Heat Mass Transf.* (1994) **37:**139–151.
[17] Wilcox, D. C., *Turbulence modeling for CFD*, 3rd ed. La Cãnada, Calif: DCW Industries, (2006).
[18] Šarler, B. and Vertnik, R. Meshfree explicit local radial basis function collocation method for diffusion problems. *Comput. Math. Appl.* (2006) **51:**1269–1282.
[19] Meeker, D. Finite element method magnetics (FEMM). 16-Oct-2010. [Online]. Available: http://www.femm.info/wiki/HomePage. [Accessed: 30-Mar-2017].
[20] Wang, B., *et al*. Analysis of the effects of electromagnetic stirring on solidification structure of bearing steel. *Metalurgija*, (2015) **54:**327–330.